Review Paper
J. Astron. Space Sci. 32(1), 13-19 (2015)
http://dx.doi.org/10.5140/JASS.2015.32.1.13

JASS Journal of Astronomy and Space Sciences

The Morphology of Equatorial Plasma Bubbles – a review

Hyosub Kil†
The Johns Hopkins University Applied Physics Laboratory, 11100 Johns Hopkins Road, Laurel MD 20723, USA

Plasma bubbles that occur in the equatorial F-region make up one of the most distinguishing phenomena in the ionosphere. Bubbles represent plasma depletions with respect to the background ionosphere, and are the major source of electron density irregularities in the equatorial F-region. Such bubbles are seen as plasma depletion holes (in situ satellite observations), vertical plumes (radar observations), and emission-depletion bands elongated in the north-south direction (optical observations). However, no technique can observe the whole three-dimensional structure of a bubble. Various aspects of bubbles identified using different techniques indicate that a bubble has a "shell" structure. This paper reviews the development of the concepts of "bubble" and "shell" in this context.

Keywords: equatorial ionosphere, irregularities, plasma bubble

1. INTRODUCTION

As the existence of an ionized layer in the upper atmosphere was verified from the radio communication through the equatorial ionosphere at the beginning of the 20th century, so too were anomalies in radio communication. The association of the radio communication anomalies with the electron density irregularities in the ionosphere was verified after the probing of the ionosphere with an ionosonde. An ionosonde is an instrument that measures the electron density as a function of height by transmitting a sweep of frequencies and receiving delayed, reflected signals from different ionospheric layers. In the absence of irregularities in the electron density, the observations of an ionosonde provide a thin-layer electron-density profile for the frequency-range coordinates. In the presence of irregularities, however, a spread in frequency or range appears in the electron density profile. The spread is caused by the irregular reflection-altitude of the transmitted signal, which indicates the existence of electron density irregularities in the reflecting layer. The spread is most severe at night in the equatorial F-region, so this phenomenon is called 'equatorial spread F' (ESF). Because of its significant effect on communication, navigation, and geodesic systems, ESF has been recognized as one of the most important space-weather features in the ionosphere.

Various terms have been used to represent the election density irregularities in the equatorial F-region. The generic name ESF originated from observations of the irregularities by ionosonde. With in situ satellite observations, irregularities appear at the places where the electron density is depleted, relative to the background ionosphere, so terms such as "depletions,", "bite-outs," and "plasma holes" were used (e.g., Hanson & Sanatani 1973, McClure et al. 1977). The terms "plumes" or "wedges" stemmed from the morphology of turbulent regions in radar observations (e.g., Woodman & La Hoz 1976, Kelley et al. 1981). "Bubble" is another generic term for the irregularities in the equatorial F-region and this name was used to reflect the generation process of the irregularities (e.g., Woodman & La Hoz 1976). Recent studies (e.g., Kil et al. 2009a) used the term "plasma depletion shell" to describe the three-dimensional (3-D) structure of bubbles.

This paper reviews the progress in our understanding of the bubble phenomenon, focusing on bubble morphology. In Section 2, the development of the "rising bubble" idea

Received Feb 23, 2015 **Revised** Mar 5, 2015 **Accepted** Mar 6, 2015
†**Corresponding Author**
E-mail: Hyosub.kil@jhuapl.edu, ORCID: 0000-0001-8288-6236
Tel: +1-240-228-6353, Fax: +1-240-228-1641

is described. Section 3 describes the mechanism by which bubbles are generated, and also provides an explanation of why bubbles occur at night in the equatorial ionosphere. In Section 4, various aspects of bubbles identified using different observation techniques, are explained using the concept of "plasma depletion shell". Section 5 concludes this paper with an unresolved issue regarding irregularities in the equatorial ionosphere.

2. EMERGENCE OF THE RISING BUBBLE MODEL

The existence of the electron density irregularities in the bottom side of the F-region was known early in the 20th century, but the mechanism by which the irregularities are generated was clarified much later. Modern study of the irregularities in the equatorial ionosphere began in the late 1960s with the emergence of in situ satellite observations, and with the observations of incoherent radar scatter at the Jicamarca Radio Observatory (JRO, 11.95° S, 76.87° W) in Peru. In situ satellite observations in the late 1960s and early 1970s identified the occurrence of plasma depletions, or plasma density holes, in the topside of the equatorial F-region at night. An interesting feature in the plasma-depleted regions was the detection of a significant fraction of molecular and metallic ions. Those ions are abundant in the lower part of the F-region, but they are rare in the topside. Fig. 1 shows the in situ measurements of the ion concentration above an altitude of 400 km by the Ogo 6 satellite (Hanson & Sanatani 1973). The square symbols connected with a line show the total ion concentration. The O^+, NO^+, and Fe^+ concentrations are indicated by plus, cross, and diamond symbols, respectively. In most regions, the square and plus symbols overlap because O^+ is the dominant ion in the topside. The peak concentrations of NO^+ and Fe^+ occurred at the bottom of the ion-depleted region. The observation of heavy ions in the topside indicates the transport of bottom side ions to the topside (Hanson & Sanatani 1973), and this idea was consistent with the radar observations of the upward plasma motion in plasma-depleted regions (McClure & Woodman 1972).

Woodman & La Hoz (1976) first introduced the idea of a rising bubble to explain the morphology of backscatter echoes in radar observations. Fig. 2a shows the backscatter power map derived from the radar observations at JRO. The power map represents the backscatter echoes produced by the electron density irregularities at a scale of 3 m. A horizontal layer of strong backscatter echoes appears near an altitude of 300 km before 2030 local time (LT). This layer is associated with the turbulence in the bottom side

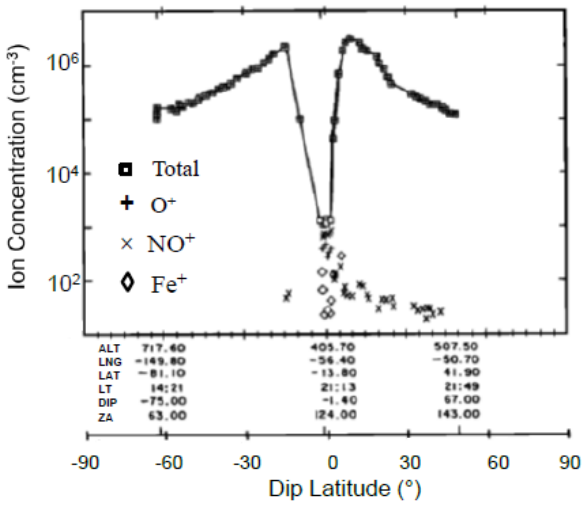

Fig. 1. In situ measurements of the ion concentration on 23 November 1969 by the Ogo 6 satellite (Hanson & Sanatani 1973). Different ion components are distinguished with different symbols, as shown in the figure. The fraction of heavy ions (NO+ and Fe+) is large at the location of total ion (and O+) depletion.

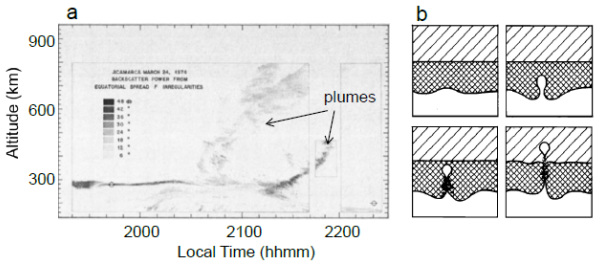

Fig. 2. (a) Backscatter power map on 24 March 1974, derived from the observation of the incoherent scatter radar at JRO. The echoes produced by rising bubbles are indicated with black arrows. (b) Schematic representation of the generation of a bubble and its propagation to higher altitudes (Woodman & La Hoz 1976).

of the F-region. Two vertical plumes of backscatter echoes appear after 2130 LT. Woodman & La Hoz (1976) explained the creation of the plumes using the schematic diagram in Fig. 2b. The three layers of different electron density represent the bottom side, near the F peak, and the topside, respectively, from the bottom to the top. The bottom layer is unstable due to gravitational Rayleigh-Taylor instability because it is located below heavy layer. A perturbation initiated in the bottom layer rises like a bubble and penetrates the top layer. The electron density irregularities exist along the trace of the bubble, as well as within and around the rising bubble. The rising bubble idea was supported by the contemporary numerical simulation study (Scannapieco & Ossakow 1976). The numerical simulation results shown in Fig. 3. demonstrate the propagation of perturbations in the bottom side to the topside, as time progresses.

The study of the bubble phenomenon blossomed in the

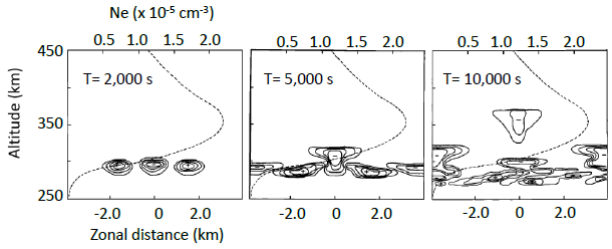

Fig. 3. Contour plots of density perturbations at 2,000 s, 5,000 s, and 10,000 s. The plus and minus signs indicate the enhancements and depletions of the electron density relative to the background. The dashed curve represents the electron density profile of the background ionosphere (Scannapieco & Ossakow 1976).

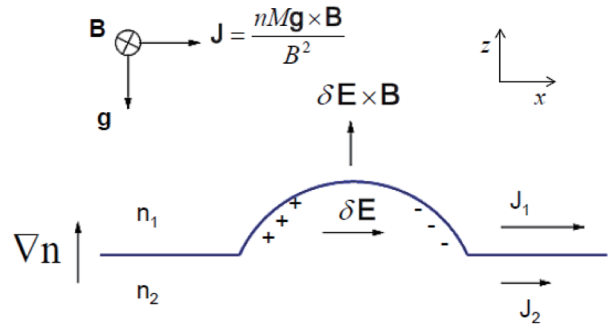

Fig. 4. Schematic illustration of the creation of a bubble by the Rayleigh-Taylor instability: The perturbation in the bottom side of the F-region induces a polarization electric field (, and the low-density bottomside plasma drifts to the (vertical) direction.

late 1970s and 1980s, and most of our current knowledge of bubbles was established during that period. The occurrence climatology of bubbles was established from long-term satellite and ground observations (e.g., Maruyama & Matuura 1984, Tsunoda 1985), and sophisticated numerical simulations could produce realistic bubble morphologies (such as tilted plumes) identified from observations (e.g., Ossakow et al. 1979, Zalesak et al. 1982). The occurrence of bubbles is affected by many factors such as local time, longitude, season, solar cycle, and geomagnetic activity. Significant progress in our understanding of the bubble activity was made through studies in the 1980s, but the variable nature of the onset condition of bubbles still remains a puzzle. We may deal with the variability of the onset condition of bubbles in a separate paper in the future.

3. CREATION OF BUBBLES BY RAYLEIGH-TAYLOR INSTABILITY

In this section, we discuss the theoretical background of the rising bubble model. The diagram in Fig. 4 schematically illustrates the process that generates a perturbation electric field. The density gradient is in the z direction ($n_1 > n_2$), and the magnetic field (**B**) is in the y direction. Under this geometry, gravitational force drives ion current (**J**) in the **g** × **B** direction (x direction). Because the current is proportional to mass (M), the electron current is negligible compared with the ion current. As the horizontal arrows indicate, more current flows in the upper layer (high-density region) than in the lower layer (low-density region). In the presence of a perturbation (half sine wave), the electron density in the upper layer is not uniform horizontally, and the current driven by gravitational force becomes discontinuous. As a result, positive and negative charges accumulate at the edges of the perturbation. Those charges induce a polarization electric field (δ **E**) and make the current continuous in the upper layer. A bubble is produced by the upward drift (δ **E** × **B**) of the plasma in the lower layer. The magnitude and persistence of the polarization electric field determines whether or not the perturbation grows into a bubble.

The linear growth rate (γ) of the perturbation in the bottom side is: $\gamma = g/(L\,\nu_{in})$ (Kelley 1989, Sultan 1996). Here g is the gravitational acceleration, ν_{in} is the ion-neutral collision frequency, and is the inverse gradient scale height of the electron number density (n) defined by $[(1/n)\ \partial n/\partial z]^{-1}$. The linear growth rate provides insight into the onset condition of a bubble. During daytime, the highly conductive E-region shorts out the polarization electric field in the F-region, so bubbles cannot develop. Thus, the linear growth rate is meaningful only at night, when the conductance in the F region is comparable to, or greater than, that in the E-region. The linear growth rate is large when the ion-neutral collision rate and the inverse gradient scale height are small. Those conditions occur just after sunset when the ionosphere is lifted to high altitudes by the phenomenon known as pre-reversal enhancement (e.g., Fejer et al. 1991, Heelis 2004). A significant portion of the variability of the bubble activity with geophysical parameters is related to the variability of the magnitude of the pre-reversal enhancement (e.g., Kil et al. 2009b).

The development of bubbles at night, especially just after sunset, can be explained by the reduction of the E-region conductance at night, and the occurrence of the pre-reversal enhancement just after sunset. Then why do bubbles develop only near the magnetic equator? The diagram in Fig. 5 illustrates the different situations at the magnetic equator and off the magnetic equator. First, let us consider the polarization electric field at the bottom side of the F-region at the magnetic equator (indicated with the letter "Q"). The reason that bubbles do not develop during daytime is that the Q-region is connected to the highly

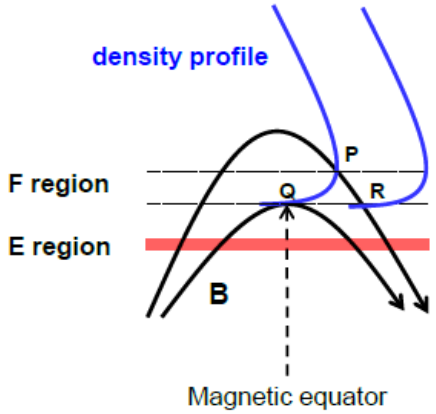

Fig. 5. Schematic illustration of the difference of the ionospheric condition at, and off, the magnetic equator.

conductive E-region along the same magnetic field line. We are now interested only in the nighttime ionosphere and can ignore the E-region. At the magnetic equator, the Q-region is not connected to a higher-density region. In other words, the polarization electric field developed at the Q-region can survive for a long time because this region is not connected to a higher conductiive region. In the diagram, electrons at the P-region cannot move to the Q-region to short out the electric field there because P-region and Q-region are not connected along the field line. The situation is different at locations off the magnetic equator. Let us assume that the region indicated with the letter "R" was perturbed and a polarization electric field developed in that region. The R-region is connected to P-region along the same magnetic field line. Because the electron density in P-region is greater than that in R-region, electrons in the P-region can short out the polarization electric field in R-region. Thus, the equatorial ionosphere is the most favorable place for the development of bubbles.

4. THREE-DIMENSIONAL BUBBLE STRUCTURE–PLASMA DEPLETION SHELL

A bubble occupies several hundred kilometers in the east-west direction, thousands of kilometers in the north-south direction, and occurs at altitudes of several hundred kilometers. This kind of large structure is not observable by any technical means on the ground or from space. However, we can construct the 3-D bubble structure by combining different parts of bubbles observed by various techniques.

As shown in Section 2, in situ satellite measurements of the ion density provide the 1-D structure of bubbles along satellite passes, and radar observations on the ground provide the 2-D (horizontal and vertical) bubble structure. With the development of an imaging system based on a charge-coupled device in 1990s, all-sky imagers have been operated around the world, for the study of the dynamics and morphology of bubbles. All-sky imagers on the ground observe nightglow emissions produced by these processes (Miller et al. 2014),

$$O^+ + O_2 \rightarrow O_2^+ + O$$

$$O_2^+ + e^- \rightarrow O(\,^1D) + O(\,^3P)$$

$$O(\,^1D) \rightarrow O + h\nu\ (630.0\ nm)$$

The intensity of the OI 630.0 nm emission is proportional to the number density of oxygen ions near an altitude of 250 km, when the O_2 concentration is constant. Because the number density of the oxygen ions inside a bubble is smaller than that in the background ionosphere, bubbles appear as emission depletions in optical observations. Because the field of view of an imager on the ground is not sufficient to cover the whole bubble image, only some portion of a bubble is visible from a ground imager.

Remote sensing of bubbles from space using far ultraviolet (FUV) sensors started with the launch of the Imager for Magnetopause-to-Aurora Global Exploration satellite in March 2000, and the Thermosphere Ionosphere Mesosphere Energetics and Dynamics (TIMED) satellite in December 2001. The FUV sensors on board those satellites observed the OI 135.6 nm nightglows, which were produced by the radiative recombination of oxygen ions. Therefore, bubbles appear as emission depletions in FUV nightglow images.

Fig. 6 shows observations of the OI 135.6 nm emission along four swaths of the Global Ultraviolet Imager (GUVI), on board the TIMED satellite on 23 March 2002 (Kil et al. 2009a). The image was projected onto the globe at an altitude of 350 km. The white horizontal dotted curve

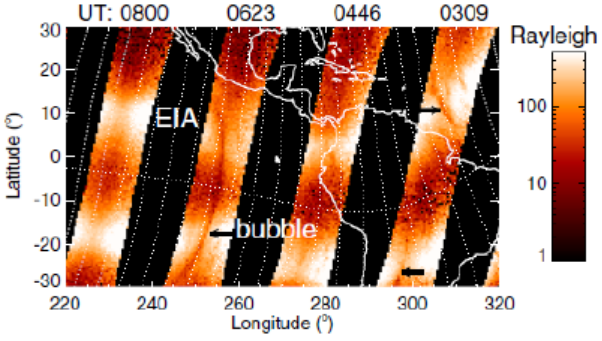

Fig. 6. OI 135.6 nm nightglow image taken on 23 March 2002 along four swaths of TIMED/GUVI: Bubble signatures are indicated with black horizontal arrows.

indicates the magnetic equator, and the white vertical dotted lines are the geomagnetic field lines. The enhanced nightglow intensity centered near ±15° magnetic latitude is produced by the equatorial ionization anomaly (EIA). As indicated with black horizontal arrows, bubbles appear as dark bands in the swaths. An arch-shape (or backward "C" shape) bubble appears between 240° E and 260° E longitudes. The bubble is elongated in the north-south direction, but its shape is not parallel to the geomagnetic field lines. As we will soon show, the backward-C shape in optical observations, and the tilt of plumes in radar observations (see Fig. 2) illustrate the same property of bubbles. In optical observations, the bubble image is dominated by the morphology at a certain height, where the contrast between the emissions in the background and plasma depleted region is significant. For this reason, the bubble structure at high altitudes is not visible from optical observations.

To explain various aspects of bubbles observed by different techniques, Kil et al. (2009a) suggested the concept of a plasma depletion shell. In Fig. 7a, a plasma depletion shell is constructed at magnetic longitude, magnetic latitude, and altitude coordinates, based on the arch-shape bubble in Fig. 6 (shown on the top of the shell structure). The black lines in the magnetic latitude-altitude plane represent dipole field lines. When a bubble develops, plasma depletion occurs in all the magnetic flux tubes in the F-region. The magnetic field lines that form the shell, indicate the plasma-depleted magnetic flux tubes. The backward-C shape image in the TIMED/GUVI observation represents the bottom part of the shell (indicated with an orange line), where the plasma depletion relative to the background is most significant. Simultaneous radar, all-sky imager, and in situ satellite observations were not available at the location and time of the TIMED/GUVI observation of the backward-C shape depletion. Here we use observations at different times and different locations to explain how the shell structure appears in those observations. Fig. 7b presents the OI 630.0 nm nightglow images observed simultaneously by the all-sky imagers in Japan and Australia (Shiokawa et al. 2004). The dark bands indicated with arrows are produced by bubbles and correspond to the pole-ward edges of the shell, as marked with blue bands. If a satellite samples the ionosphere by crossing the shell at

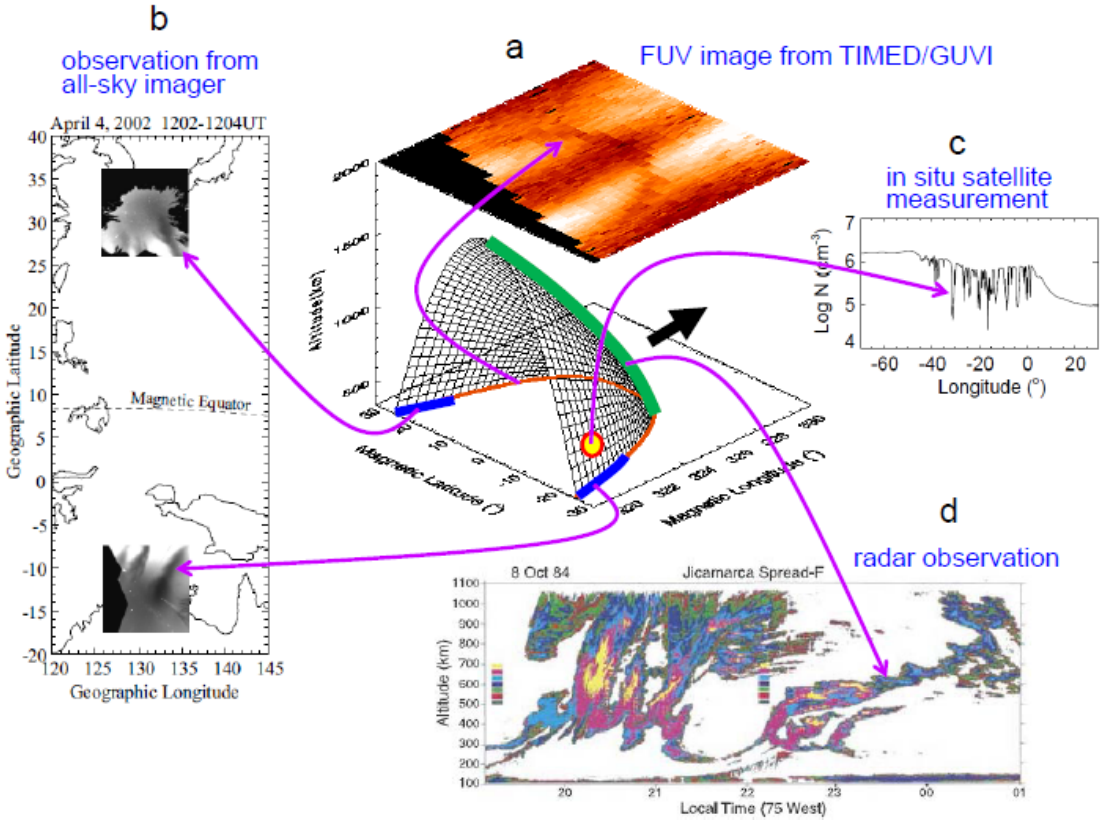

Fig. 7. Various aspects of bubbles observed using different techniques: (a) Plasma depletion shell produced on the basis of the arch-shaped bubble in Figure 6 (shown on the top of the shell structure). The black arrow indicates the eastward drift of the shell structure (Kil et al. 2009a). (b) OI 630.0 nightglow images observed simultaneously in Japan and Australia on 4 April 2002 (Shiokawa et al. 2004). (c) In situ measurements of the ion density by the first satellite of the Republic of China on 22 September 2002. (d) Backscatter power map observed by the incoherent scatter radar at JRO on 8 October 1984 (Kelley et al. 2003).

the location of the yellow dot, it detects a depletion of the ion density as shown in Fig. 7c. Normally, the ionosphere and bubbles drift eastward at night. The black thick arrow in Fig. 7a indicates the eastward drift of the shell structure. A vertically pointing radar at the magnetic equator can detect the shell at the magnetic equator (marked with a green band in Fig. 7a). The radar first observes the bottom part of the shell, and then it observes the shell at higher altitudes as the shell passes by (or as time progresses). The tilted plumes in the radar observation shown in Fig. 7d (Kelley et al. 2003) correspond to the observation of the back of the shell, as marked with the green band.

Formation of the shell structure is associated with the differential zonal drift of plasmas in different magnetic flux tubes. The diagram in Fig. 8 schematically illustrates this process (Kil et al. 2009). The diagram assumes the development of a vertically upright bubble at $t = 0$. Plasma is depleted in the region indicated with gray. The gray region is filled with plasma-depleted flux tubes. As examples, four magnetic flux tubes are indicated with thick lines. Plasmas in a magnetic flux tube drift with the same velocity, in the zonal direction. The horizontal arrows represent differential eastward drifts of plasmas in different magnetic flux tubes. The innermost flux tube drifts fastest and the outermost flux tube drifts slowest. Later (t = T), plasmas in different flux tubes occupy different longitudes owing to their differential zonal velocity. The morphology of the bubble represented with the plasma-depleted magnetic flux tubes at t = T is the same as the shell structure in Fig. 7a. If the zonal drift velocity is uniform, the optical signature of the bubble is a straight emission depletion band elongated in the north-south direction.

The zonal plasma drift is driven by vertical electric fields. The altitudinal and latitudinal difference of the zonal plasma drift velocity indicates the variation of the vertical electric field with altitude and latitude. The magnitude of the vertical electric field is determined by the combined effects of the conductivities in the E and F regions, and the zonal, neutral wind velocity (Zalesak et al. 1982, Anderson & Mendillo 1983, Huba et al. 2008). Huba et al. (2008) identified the formation of a plasma depletion shell in association with the variation of the zonal wind velocity, by conducting model simulations. The shell structure was also identified from the azimuth distribution of the fluctuation in total electron content (TEC, Park et al. 2015). The fluctuation in TEC is more significant when the TEC is measured along the shell structure, rather than across the shell structure.

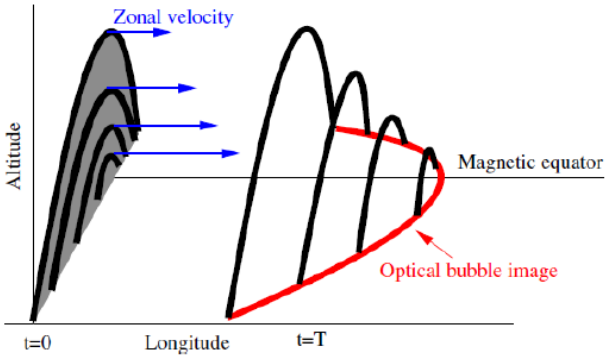

Fig. 8. Schematic illustration of the formation of a plasma depletion shell structure by the differential zonal drift of plasmas in different magnetic flux tubes (Kil et al. 2009a).

5. CONCLUSIONS

As reviewed in previous sections, the mechanism by which bubbles are generated, and their morphology, are well understood. Recent studies of the bifurcation and merger of bubbles may provide a comprehensive understanding for the evolution of the bubble morphology. Currently, the most challenging issue regarding the bubble phenomenon is the variability of the onset condition of bubbles, which is affected by a number of factors. Understanding the onset condition of bubbles is essential for prediction of the occurrence of bubbles. Several hypotheses have been proposed to explain the onset condition of bubbles, but the highly variable nature of the bubble activity is not described satisfactorily by any one hypothesis, or even by all the hypotheses together. Because multiple factors appear to affect the creation of bubbles, observations of various components simultaneously using different techniques are desirable. At the same time, worldwide long-term observations are necessary to acquire accurate knowledge of the occurrence climatology of bubbles.

ACKNOWLEDGEMENTS

H. Kil acknowledges support from National Science Foundation Aeronomy program (AGS-1237276).

REFERENCES

Anderson DN, Mendillo M, Ionospheric conditions affecting the evolution of equatorial plasma depletions, GRL 10, 541-544 (1983). http://dx.doi.org/10.1029/GL010i007p00541

Fejer BG, de Paula ER, González SA, Woodman RF, Average vertical and zonal F region plasma drifts over Jicamarca,

JGR 96, 13901-13906 (1991). http://dx.doi.org/10.1029/91JA01171

Hanson WB, Sanatani S, Large Ni gradients below the equatorial F peak, JGR 78, 1167-1173 (1973). http://dx.doi.org/10.1029/JA078i007p01167

Heelis RA, Electrodynamics in the low and middle latitude ionosphere: a tutorial, JASTP 66, 825-838 (2004). http://dx.doi.org/10.1016/j.jastp.2004.01.034

Huba JD, Joyce G, Krall J, Three-dimensional equatorial spread F modeling, GRL 35, L10102 (2008). http://dx.doi.org/10.1029/2008GL033509

Kelley MC, Larsen MF, LaHoz C, McClure JP, Gravity wave initiation of equatorial spread F: A case study, JGR 86, 9087-9100 (1981). http://dx.doi.org/10.1029/JA086iA11p09087

Kelley MC, The Earth's Ionosphere (Academic Press, San Diego, 1989).

Kelley MC, Makela JJ, Paxton LJ, Kamalabadi F, Comberiate JM, et al., The first coordinated ground- and space-based optical observations of equatorial plasma bubbles, GRL 30, 1766 (2003). http://dx.doi.org/10.1029/2003GL017301

Kil H, Heelis RA, Paxton LJ, Oh S-J, Formation of a plasma depletion shell in the equatorial ionosphere, JGR 114, A11302 (2009a). http://dx.doi.org/10.1029/2009JA014369

Kil H, Paxton LJ, Oh S-J, Global bubble distribution seen from ROCSAT-1 and its association with the evening prereversal enhancement, JGR 114, A06307 (2009b). http://dx.doi.org/10.1029/2008JA013672

Maruyama T, Matuura N, Longitudinal variability of annual changes in activity of equatorial spread F and plasma bubbles, JGR 89, 10903-10912 (1984). http://dx.doi.org/10.1029/JA089iA12p10903

McClure JP, Woodman RF, Radar observations of equatorial spread F in a region of electrostatic turbulence, JGR 77, 5617-5621 (1972). http://dx.doi.org/10.1029/JA077i028p05617

McClure JP, Hanson WB, Hoffman JH, Plasma bubbles and irregularities in the equatorial ionosphere, JGR 82, 2650-2656 (1977). http://dx.doi.org/10.1029/JA082i019p02650

Miller ES, Kil H, Makela JJ, Heelis RA, Talaat ER, et al., Topside signature of medium-scale traveling ionospheric disturbances, Ann. Geophys. 32, 959-965 (2014). http://dx.doi.org/10.5194/angeo-32-959-2014

Ossakow SL, Zalesak ST, McDonald BE, Chaturvedi PK, Nonlinear equatorial spread F: Dependence on altitude of the F peak and bottomside background electron density gradient scale length, JGR 84, 17-29 (1979). http://dx.doi.org/10.1029/JA084iA01p00017

Park J, Lühr H, Noja M, Three-dimensional morphology of equatorial plasma bubbles deduced from measurements onboard CHAMP, Ann. Geophys. 33, 129-135 (2015). http://dx.doi.org/10.5194/angeo-33-129-2015

Scannapieco AJ, Ossakow SL, Nonlinear equatorial spread F, GRL 3, 451-454 (1976). http://dx.doi.org/10.1029/GL003i008p00451

Shiokawa K, Otsuka Y, Ogawa T, Wilkinson P, Time evolution of high-altitude plasma bubbles imaged at geomagnetic conjugate points, Ann. Geophys. 22, 3137-3143 (2004). http://dx.doi.org/10.5194/angeo-22-3137-2004

Sultan PJ, Linear theory and modeling of the Rayleigh-Taylor instability leading to the occurrence of equatorial spread F, JGR 101, 26875-26891 (1996). http://dx.doi.org/10.1029/96JA00682

Tsunoda RT, Control of the seasonal and longitudinal occurrence of equatorial scintillations by the longitudinal gradient in integrated E region Pedersen conductivity, JGR 90, 447-456 (1985). http://dx.doi.org/10.1029/JA090iA01p00447

Woodman RF, La Hoz C, Radar observations of F region equatorial irregularities, JGR 81, 5447-5466 (1976). http://dx.doi.org/10.1029/JA081i031p05447

Zalesak ST, Ossakow SL, Chaturvedi PK, Nonlinear equatorial spread F: The effect of neutral winds and background Pedersen conductivity, JGR 87, 151-166 (1982). http://dx.doi.org/10.1029/JA087iA01p00151